2017-07-01

Using Advanced PSF Subtraction Techniques on Archival Data of Herbig Ae/Be Stars to Search for New Candidate Companions

Emily Diane Safsten
Brigham Young University

Using Advanced PSF Subtraction Techniques on Archival Data of Herbig Ae/Be Stars to Search for New Candidate Companions

Emily Diane Safsten

A thesis submitted to the faculty of
Brigham Young University
in partial fulfillment of the requirements for the degree of

Master of Science

Denise Stephens, Chair
Michael Joner
Darin Ragozzine

Department of Physics and Astronomy

Brigham Young University

ABSTRACT

Using Advanced PSF Subtraction Techniques on Archival Data of Herbig Ae/Be Stars to Search for New Candidate Companions

Emily Diane Safsten
Department of Physics and Astronomy, BYU
Master of Science

Herbig Ae/Be (HAeBe) stars are intermediate mass (2-10 solar mass) pre-main sequence stars with circumstellar disks. Observing planets within these young disks would greatly aid in understanding planet formation processes and timescales particularly around massive stars. So far, only one planet, HD 100546 b, has been confirmed to orbit a HAeBe star. With over 250 HAeBe stars known, and several observed to have disks with structures thought to be related to planet formation, it seems likely that there are as yet undiscovered planetary companions within the circumstellar disks of some of these young stars.

Direct detection of a low-luminosity companion near a star requires high contrast imaging, often with the use of a coronagraph, and the subtraction of the central star's point spread function (PSF). Several processing algorithms have been developed in recent years to improve PSF subtraction and enhance the signal-to-noise of sources close to the star. However, many HAeBe stars were observed via direct imaging before these algorithms came out. We used the PSF subtraction program PynPoint to reprocess archival images of HAeBe stars from the Advanced Camera for Surveys on the Hubble Space Telescope to increase the likelihood of detecting a planet in their disks. We believe we have recovered the known planet around HD 100546 and possibly its candidate second companion. We also detect new candidate sources in the vicinities of HD 141569 and HD 163296. Further observations are needed to confirm the reality of these detections and also establish their association with the host stars.

Keywords: PSF subtraction, Herbig Ae/Be stars, Hubble ACS data

ACKNOWLEDGMENTS

My thanks and appreciation first and foremost go to my advisor, Dr. Denise Stephens, for her support of this project (financial and otherwise) and for all she has taught me. Thanks to the Department of Physics and Astronomy at BYU for funding this research as well. I'd also like to thank Leanne Lunsford for performing an archival search for HAeBe stars. Many thanks go to Mario van den Ancker, Mario Perez, Davide Fedele, and David Golimowski for being willing to collaborate on telescope proposals. Even though we were never granted time, it was still a good experience and I very much appreciate their help. Additional thanks go to Mario Perez for his suggestions that led me to the idea for this project. And of course, thanks to my husband Alex for his support and encouragement.

Contents

List of Figures

Chapter 1

Introduction

1.1 Planets and Circumstellar Disks

The planets in our solar system have long been theorized to have formed from coalescence and accretion of material within a disk of gas and dust surrounding the nascent Sun. This theory has of course been modified over the years to explain the details of our solar system's particular configuration. But only relatively recently have we been able to compare this theory with observations of systems other than our own. The Hubble Space Telescope (HST) spotted stars in the Orion Nebula surrounded by dark disks (McCaughrean & O'dell 1996), and disks of material have been found around many stars in the sky, either observed directly or inferred by excess infrared (IR) emission from the star. These validate our ideas about the origin of our planetary system. The Kepler space telescope (Borucki et al. 2010) and other exoplanet surveys have also revealed a multitude of planetary systems, many of which differ greatly from our own and thus challenge planet formation theories.

Examination of the database of known exoplanets (http://exoplanetarchive.ipac.caltech.edu) shows that the vast majority of these worlds have been found around stars of spectral type F or later.

This is understandable for several reasons. In our search for other habitable worlds, it makes sense to focus on the stars that are more similar to the Sun, as we know that they can host Earthlike planets. It is also easier to confirm planets around solar mass or smaller stars than larger ones. Stars that are massive and bright make it more difficult to detect the subtle change in brightness from a planetary transit. In addition, massive stars are often variable and/or rapid rotators, which broadens their spectral lines and makes planet detection via radial velocity difficult. Massive stars are also less common than smaller stars. This leaves the census of planets around more massive stars relatively sparse, and it is not yet clear if this is because planets tend not to form around massive stars, or if it is just an observational bias.

Recent research is starting to find more planets around hot stars using a new technique called Doppler tomography. This involves studying the change in the shape of the spectral line profiles as a planet transits a star, going from the redshifted to the blueshifted part of the star. With this method, the KELT team has detected five hot Jupiters orbiting A stars; this is 25% of the hot Jupiters they have found thus far (Gaudi et al. 2017). These results are showing that planets around massive stars are indeed there and may even be plentiful.

Studying these stars and their environments at their earliest stages can help in answering this question further. Our current understanding of star and planet formation suggests that each star will have a circumstellar disk of gas and dust for a period early in its life. As described in Williams & Cieza (2011), the first phase of this is called the primordial disk stage, when the circumstellar material makes a continuous disk of gas and dust around the star. As planets form, they may clear out gaps in the disk while an inner hole forms as the star photoevaporates the gas and pushes it out of the disk (Williams & Cieza 2011). This is the transition disk, so called because it is the stage between the primordial disk and the final phase, known as the debris disk. This last stage is when the gas has been cleared out and all that are left are planets, planetesimals, and dust (Williams & Cieza 2011). Since all stars should have circumstellar disks, it seems plausible that most if not all

stars will end up with a planetary system, and the new KELT results lend support to this notion. Studying disks and very young planets reveals clues to how these systems form. Most circumstellar disks of young stars known to host planets are in the debris disk stage. Because planets are growing during the transition disk phase, observing planets at this stage would place important constraints on formation timescales and the masses of planets that can form. Thus, we are most interested in detecting planets within these transition disks.

Often the structure of a circumstellar disk is inferred by the nature of IR emission from the region of the star, but some disks can be observed directly (Williams & Cieza 2011). Some of these directly imaged disks exhibit asymmetries in their structure that are thought to be induced by planets (Williams & Cieza 2011). Some asymmetrical structures may be dust traps or vortices, which could be important in forming planets (Cieza 2016). Additionally, multiple young stars show spiral arms in their circumstellar disks, similar to the spiral structure of many galaxies. According to Fung & Dong (2015), multiple planets in the disk, or even a single massive planet, may induce multiple arms as they excite density waves in the disk that produce the spirals. Studying these can reveal disk and planet properties, such as the mass of the planet (Fung & Dong 2015). Thus, even if planets in disks have not yet been observed directly, their presence can often be inferred from the structure of the disk itself.

1.2 Planets around HAeBe Stars

Because of the difficulties in detecting planets around massive stars combined with the presence of circumstellar material obscuring planetary signatures, the best way to find these young planets is to observe the systems directly. Young intermediate mass stars (approximately 2-10 solar masses) that still have gas and dust disks are called Hebig Ae/Be (HAeBe) stars, and are of spectral type B, A, and sometimes F. Stars at this stage that are solar mass and smaller are called T Tauri stars. T Tauri

stars are fairly well studied and give us a glimpse into what our solar system was like in its earliest stages. But the HAeBe stars are not as well understood because they are less common.

There have been a few planets confirmed around young stars (e.g. LkCa15 b, Kraus & Ireland 2012; HD 95086 b, Rameau et al. 2013), but so far, only one planet has been confirmed around a HAeBe star. The host star, HD 100546, is one of the closest HAeBe stars, and its circumstellar environment has been well studied in a variety of wavelength regions. Its disk is known to have spiral arms and a gap in the inner region of the disk (e.g. Ardila et al. 2007; Benisty et al. 2010; Grady et al. 2001). However, a planet was not detected until the system was observed in the L' filter ($\lambda = 3.8\mu$m) by Quanz et al. (2013). They performed coronagraphic imaging of HD 100546 in L' with the NACO instrument on the Very Large Telescope (VLT) and clearly detected an emission source in the disk. The source was confirmed to be a planet by Quanz et al. (2015), who observed it with the same equipment in L', M' ($\lambda = 4.8\mu$m), and K_s ($\lambda = 2.1\mu$m) filters. They detected the planet in L' and M', but not K_s. It was not detected at shorter wavelengths until Currie et al. (2015) performed high-contrast imaging of the system in H band ($\lambda = 1.6\mu$m) with the Gemini Planet Imager. The young planet, which orbits at a distance of about 53 AU from its star, has a temperature of about 932 K and is several times the size of Jupiter (Quanz et al. 2015). The image from Quanz et al. (2015) showing the planet in the disk of HD 100546 is given in Figure 1.1.

There are probably many planets in the circumstellar disks of HAeBe stars that have not been detected yet simply because they have not been observed in the right filters or with high enough contrast. A planet with a temperature of 900 or 1000 K would emit most of its radiation right in the range of the L band (3-4 μm), and at tens of AU away from the central star, the disk emission in this region would drop off significantly. This would provide a high contrast between a planet and the surrounding material, enabling the planet to show up much more easily while it is undetectable in other wavelength ranges. Additionally, it is only relatively recently that the technology needed for directly imaging planets has become available. This includes not only high-quality instruments but

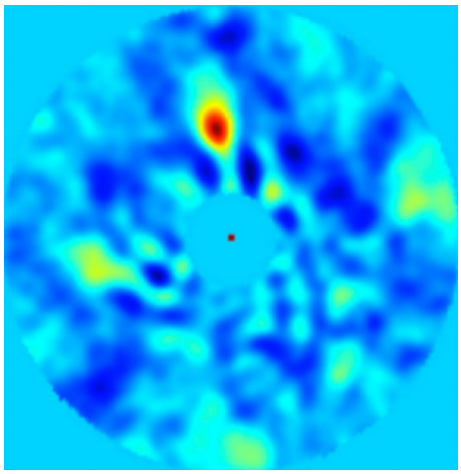

Figure 1.1 L' image from Quanz et al. (2015) showing the planet (red spot) in the disk of HD 100546.

also post-processing algorithms, which will be described in later sections. Planets found in these disks would be quite interesting because they would be very young, possibly still forming. Studying their mass, luminosity, composition, and location in the disk would greatly aid in understanding planet formation around higher mass stars.

1.3 Coronagraphic Imaging and PSF Subtraction

Stars are so far away that even the closest ones are basically point sources of light. However, during telescopic observations, the starlight gets diffracted by the optics of the telescope system and, for ground-based instruments, refracted by the Earth's atmosphere. This results in what is called a point spread function, or PSF, in which the starlight is spread over several pixels in the image. The light is concentrated in the center of the PSF, but it also has wings that extend out from this core. Any planets or circumstellar material around the star of interest are much dimmer than their host and will get lost in this glare.

One way to mitigate this problem is by using a coronagraph. This is a dark mask that is placed in front of part of the detector and used to block the light from a bright star. This helps nearby sources

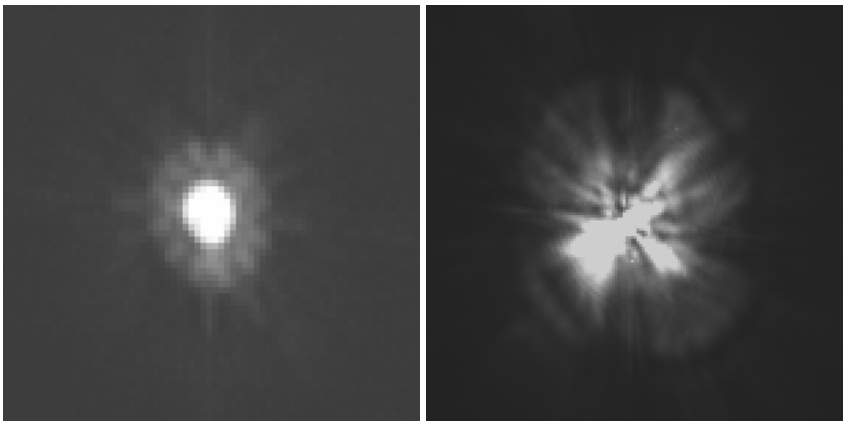

Figure 1.2 ACS PSFs without (left) and with (right) a coronagraphic mask in place. Due to different exposure times, the brightness scales are not the same; what is important to note is the shape of the PSFs.

to show up better, but light from the central star is still scattered about the mask. Close companions can still get lost in the PSF amidst the so-called speckles that occur, which are long-lived bright spots primarily resulting from instrumental imperfections (Lafrenière et al. 2007). As examples, images taken with and without a coronagraphic spot on HST's Advanced Camera for Surveys (ACS) are given in Figure 1.2.

To see sources and material close to the star, one must subtract off the PSF of the target of interest. Classically, this has been done by observing another star of the same color as the target and subtracting its PSF from that of the target star. Various observing techniques have been developed over the years to improve this PSF subtraction by taking advantage of the quasi-static nature of the speckles. These include angular differential imaging (Marois et al. 2006), simultaneous spectral differential imaging (Marois et al. 2000; Racine et al. 1999), and polarimetric differential imaging (Kuhn et al. 2001), to name a few. While these methods do help, the speckles are not completely stationary and suffer from variations due to temperature changes, guiding errors, and small aberrations within the camera (Lafrenière et al. 2007). This means that the PSF that is subtracted off is usually not highly correlated with the actual PSF, and the subtraction will still leave

behind enough noise to obscure a planet.

Within the past decade or so, several algorithms have been developed to construct a model PSF from a set of reference images and thus produce a much more accurate subtraction. One of the best known of these is the LOCI algorithm (Lafrenière et al. 2007). Other examples include KLIP (Soummer et al. 2012) and PynPoint (Amara & Quanz 2012; Amara et al. 2015), which both make use of a method of principal component analysis. But since these are somewhat recent developments, a lot of older data have not had the advantage of these new methods.

Images acquired before these algorithms were developed may thus be reprocessed using advanced techniques to reveal previously unseen features, or confirm and provide more information about known sources. The potential effectiveness of this method is demonstrated by Choquet et al. (2014). They have developed an advanced PSF subtraction pipeline called ALICE which they are using to reprocess the entire coronagraphic archive of HST's NICMOS instrument. This has already revealed many point sources, and resolved five debris disks in the infrared for the first time (Choquet et al. 2014). Other datasets may similarly reveal important and interesting results.

1.4 Research Goal

The goal of this project was to detect previously unknown planetary mass companions around HAeBe stars. We twice submitted proposals to use VLT/NACO to coronagraphically image several targets of interest in the L' band, as this seems to be the optimal wavelength range in which to detect young, forming planets as described above. Since we were not granted telescope time, we instead undertook a reprocessing of archival coronagraphic data from HST using the program PynPoint to try to detect any previously missed companions. In the following chapters and sections, we will describe the dataset we used, the specifics of the PSF subtraction program employed, the results of our work, and what we hope to do in the future.

Chapter 2

Individual Targets and ACS Data

2.1 Herbig Ae/Be Stars of Interest

There are over 250 HAeBe stars known (Chen et al. 2016), but of course some of these are much more conducive for finding young planets than others. In this section we discuss in more detail the particular stars we examined and why they are good candidates for hosting newly formed companions.

There are several reasons why we selected these stars. First, the stars we are interested in are relatively close, making it easier to detect faint close companions. Their disks have moderate to low inclinations, i.e. not edge-on (0° inclination is a face-on system). While it is possible to detect planets in edge-on systems like Beta Pictoris (Lagrange et al. 2009; Smith & Terrile 1984), face-on systems are preferred for direct imaging because there is less material in the way and the planets can be observed at any point in their orbits. Finally, our HAeBe targets have been previously reported to have holes, gaps, and/or spiral arms. As discussed earlier, these structures indicate the evolution of the disk and the possible influence of planetary bodies.

We had a list of nine HAeBe targets that we proposed to observe with VLT – six for each

proposal with three overlapping – as well as some other targets of interest not included in the proposals due to time or coordinate constraints. Since we did not get the telescope time desired, we undertook a search for these stars in the archives of several telescopes, including HST, Keck, Gemini, Spitzer, and Herschel. This yielded fairly fruitful results. Six stars that we are interested in, including five that were on our VLT proposals, had been observed with a coronagraph on the ACS instrument on HST in the F606W filter. We decided to reanalyze these images using advanced PSF subtraction to see if we could detect anything that had been missed before.

We discuss in more detail some of the targets we are interested in. This is not an exhaustive list, but rather only covers those which had images in the dataset we used. We discuss the dataset itself in the next section.

2.1.1 HD 34282

This is a star with a temperature of 8625 K, an age of 6.4 Myr, and spectral type estimates ranging from A0V to A3V (Alecian et al. 2013; Merín et al. 2004). It is also known to be a short-period variable star of the δ Scuti type (Amado et al. 2004; Casey et al. 2013). Estimates for the distance to HD 34282 have varied greatly, from the Hipparcos value of 164 pc to the estimate of 400 pc by Piétu et al. (2003) based on other stellar parameter values. Using the Hipparcos parallactic distance, van den Ancker et al. (1998) derived stellar parameters for HD 34282, but these placed the star in an anomalous position on the HR diagram. The value of 348 pc from Merín et al. (2004), as well as the estimate by Piétu et al. (2003), give the star properties closer to those expected for its spectral type. The recent Gaia data release (Lindegren et al. 2016) gives a parallax for HD 34282 that implies a distance of 325 pc, lending credence to the later estimates.

Piétu et al. (2003) first resolved the disk of HD 34282 in CO emission, and Dent et al. (2005) found the disk inclination to be $50 \pm 5°$. The work of Khalafinejad et al. (2016) indicates the presence of a large dust gap in the disk, suggestive of the influence of planet formation and that the

disk is in the transitional stage. However, recent infrared observations in H band by Uyama et al. (2017) detected no companions to this star.

2.1.2 HD 97048

HD 97048 is a well-studied HAeBe star of spectral type A0 and temperature 10000 K located about 175 pc away (Keller et al. 2008; van Boeckel et al. 2005; van den Ancker et al. 1998). Its disk has been resolved in multiple wavelengths and extends to hundreds of AU (e.g. Acke & van den Ancker 2006; Habart et al. 2004). Using infrared images, Lagage et al. (2006) determined the disk inclination to be 42.8° and the age of the system to be about 3 Myr.

Maaskant et al. (2013) reported the detection of a gap in the disk of HD 97048, stretching from 2.5–34 AU. Walsh et al. (2016) and Ginski et al. (2016) both found ring and gap structures. Similar morphology as well as a large dust cavity were observed by van der Plas et al. (2017), who estimate that a gas giant planet of $\approx 0.7\ M_{\rm jup}$ could open up the cavity.

2.1.3 HD 100453

This is an A9Ve star (Houk & Cowley 1975) located at about 103 pc (Gaia Collaboration 2016). Its disk is thought to be transitioning from a gas-rich protoplanetary disk to a gas-poor debris disk (Collins et al. 2009). Wagner et al. (2015) discovered a two-armed spiral structure as well as dark regions which they interpret to be a gap possibly caused by planets, and further work by Khalafinejad et al. (2016) suggests the presence of a gap in the disk extending from about 1 AU to 20 AU. Long et al. (2017) found that the outer disk is inclined at 25°, and Collins et al. (2009) estimate the age of the system to be 8-12 Myr.

HD 100453 has an M-dwarf companion, HD 100453B, located 120 AU from the central star (Chen et al. 2006). Dong et al. (2016) showed that this object may be responsible for the observed spiral arm structure in the disk. Collins et al. (2009) also found a faint source at a radius of ~ 0.8”

which they referred to as star C, but concluded that this is a background star as it does not share common proper motion with HD 100453A and B.

2.1.4 HD 100546

This is one of the closest HAeBe stars, at 109 pc away (Lindegren et al. 2016), and has been studied extensively over the years. It is a B9Vne star (Levenhagen & Leister 2006) with a temperature of about 10500 K and age of about 10 Myr (Guimarães et al. 2006; van den Ancker et al. 1997).

The large (r > 300 AU, e.g. Augereau et al. 2001; Pantin et al. 2000) disk of HD 100546 is inclined at 42° (Pineda et al. 2014) and has a complex structure that has been observed with a variety of instruments from optical to millimeter wavelengths (e.g. Ardila et al. 2007; Augereau et al. 2001; Grady et al. 2001). It exhibits asymmetries, spiral arms, and an inner gap that may be induced by planets (e.g. Ardila et al. 2007; Benisty et al. 2010; Grady et al. 2001).

HD 100546 is the only HAeBe star so far confirmed to have a planet in its disk, a Jovian planet at about 50 AU with extended emission that may be a circumplanetary disk (Quanz et al. 2015). There is also an unconfirmed second planet "c" at 14 AU (Currie et al. 2015) that may be related to the observed hole in the inner part of the disk, which spans from a few AU to about 14 AU (Quanz et al. 2015, and references therein). Multiwavelength observations of these young companions will shed much light on their formation processes and interactions with the disk.

2.1.5 HD 141569

HD 141569 is a well-studied B9.5 Ve star located about 116 pc away (Folsom et al. 2012; Juhász et al. 2010) which is actually part of a triple star system. It has two M-dwarf companions in a binary system located about 7.5" away (Weinberger et al. 2000). Multiple observations have revealed a large disk (r > 400 AU) with ring structures located at 325 AU and 200 AU (e.g. Augereau et al. 1999; Mouillet et al. 2001; Weinberger et al. 1999). This disk is inclined at about 51° (Weinberger

et al. 1999). Additional observations have shown that there is an inner ring and an inner disk with radius of 39 AU (Currie et al. 2016). The outer disk also exhibits spiral arms, which may be due to the stellar companions or the influence of unseen planets (Biller et al. 2015; Seok & Li 2017).

The disk of HD 141569 is optically thin with significant clearing of material, but it still has a substantial amount of gas (Merín et al. 2004). This means it is near the end of the transitional stage and will soon be a debris disk. The estimated age for the system is 5 ± 3 Myr (Weinberger et al. 2000).

2.1.6 HD 163296

HD 163296 is another close, well-studied star of spectral type A1Ve (Juhász et al. 2010). It is about 122 pc away (van den Ancker et al. 1998). Many observations (e.g. Fukagawa et al. 2010; Grady et al. 2000) report a resolved disk extending out to 540 AU and inclined at 46° (Isella et al. 2007). van den Ancker et al. (1998) estimate an age of 5 Myr for the system.

Ring and gap structures have been observed in the disk, including a ring at 77 AU (Garufi et al. 2014; Monnier et al. 2017) and evidence for a ring at 96 AU (Guidi et al. 2016). Recently, Isella et al. (2016) found several gaps in the disk, located at 60, 100, and 160 AU. In the middle and outer gaps, they observed a depletion of both gas and dust, which they suggest could be a result of Saturn-mass planets orbiting within the gaps.

2.2 Archival Coronagraphic ACS Images

We found that the targets discussed above had all been coronagraphically observed with the Advanced Camera for Surveys (ACS) on HST. The ACS is a visible-to-near infrared photometric imager that became operational in the early 2000s. It has two coronagraphic spots, one of 0.9"-radius and the other of 1.5"-radius. Its data is accessible via the HST MAST archive at

http://archive.stsci.edu/hst/.

To our knowledge, based on literature searches, no one has processed these images with advanced PSF subtraction algorithms to look for new point sources. We downloaded all the available 0.9"-coronagraphic ACS data taken in the F606W filter with the High Resolution Channel (HRC), which has a plate scale of $\sim 0.028" \times 0.025"$/pixel.

The F606W filter is centered at 606 nm, which is red visible light and similar to the more standard R filter. A far cry from L', this is not the ideal wavelength at which to observe planets, as such objects are cold enough that they emit extremely little visible light. The infrared NICMOS data would have been preferrable, but the ALICE group is already working with that. However, even though the objects we hope to find produce almost no visible light of their own, they will still reflect light from their host stars. So it may be possible to see them in optical data. And as most direct imaging searches focus on detecting thermal emission from the planets, observing them in reflected light would add another dimension to understanding these objects that seems to be as yet quite unexplored.

ACS suffers from a geometric distortion. This is primarily due to its optical design, constructed to correct for spherical aberrations (Avila et al. 2017). The distortion manifests itself in a stretching of the images along a diagonal. This is not really problematic for the PSF subtraction, since each image is affected in the same way. However, care should be taken when processing images acquired at different orientations. Subtraction programs will typically rotate the science images to the same angle, and in a distortion-affected dataset, this means that point source companions and other features will not properly line up.

From the archive, the user can download images from various stages of reduction and processing. These stages are distinguished by extensions in the file names. Images with crj have been calibrated and cosmic ray-cleaned, but not corrected for the geometric distortion. There are distortion-corrected images, with extension drz, but these are not cosmic ray-cleaned. Cosmic rays can look very much

like real point sources, and we opted to use the crj images for this project.

We individually examined each image downloaded in order to remove bad frames. Bad frames include those in which the coronagraph clearly did not successfully cover a star, as well as those that were strongly saturated and thus varied significantly from the normal PSF. These were removed from the data set and not used further.

Chapter 3

PynPoint

3.1 Why PynPoint

We originally looked into a few different implementations of various PSF subtraction algorithms to use for this project. These included PynPoint, a program called pyKLIP which uses a KLIP algorithm (Wang et al. 2015), and a program called VIP which uses a method of local low-rank plus sparse plus Gaussian-noise decomposition (LLSG; Gomez Gonzalez et al. 2016). Ideally, it would be nice to use all these techniques to try to confirm results with multiple methods, although the pyKLIP program is a bit limited because it only has modules for instruments on Keck and GPI. But given time constraints, that is beyond the scope of this work.

Amara & Quanz (2012) demonstrate the effectiveness of PynPoint and its better performance compared to another PSF subtraction method called LOCI. They show that PynPoint is significantly better at detecting planets, particularly planets close to the central star. This was also the first of the programs which we really learned how to use, and we settled on working with it because of its ease of use, effectiveness, and versatility in being applied to data from a variety of instruments.

We describe here the basics of using the program and refer the reader to the PynPoint website

(http://pythonhosted.org/PynPoint-exoplanet/index.html) for more thorough instructions for its use.

3.2 How It Works

The PynPoint program, described in Amara & Quanz (2012) and Amara et al. (2015), is an advanced PSF subtraction program that uses a method of principal component analysis (PCA). As described in the tutorial by Smith (2002), the basic idea of PCA is to reconstruct the dataset in terms of one or more of the eigenvectors of the covariance matrix of the mean-subtracted data. This reconstruction helps show how each individual point relates to the rest of the data (Smith 2002). The eigenvector with the highest eigenvalue is the principal component of the dataset and represents the strongest relationship within the data (Smith 2002). The more eigenvectors included in the reconstruction, the more information about data relationships is included, but the amount added decreases with smaller and smaller eigenvalues (Smith 2002).

PynPoint constructs a model PSF for the images in question from a linear combination of a set of basis images (Amara & Quanz 2012). The basis images can consist of any frames taken with the same setup as the target, including the target itself. The most important parameter in PynPoint for producing a good PSF subtraction is the number of PCA coefficients used. This is essentially the number of basis images that are used to model the PSF. Hence, the number of PCA coefficients available ranges from 1 up to the number of images in the basis. The greatest improvements in the subtraction come within the first several tens of coefficients, after which the change is usually relatively marginal.

The user defines two sets of images as instances of the `images` class and the `basis` class (Amara et al. 2015). The `images` class contains the data for the target of interest. The `basis` class contains the images used to construct the model PSF. A `residuals` class is also used. This tells PynPoint what basis and what images to use and is then used to plot what is left over when the model PSF is

subtracted off the images, averaged through the image stack (Amara et al. 2015). All the instances being defined, the user can then specify the number of PCA coefficients to use and instruct PynPoint to produce the resulting residuals image.

An important piece of information that PynPoint will look for in the headers of the images is their parallactic angle (Amara et al. 2015). This is the angle between the line connecting the target to the north celestial pole and the line connecting the target to the zenith. For a space telescope such as Hubble, this is meaningless. Instead, we use the telescope's orientation angle, which is the position angle – how far east of north – of the y-axis of the image. The shape of the PSF does not depend on the parallactic or orientation angle, but the apparent location of a nearby companion does. A technique called angular differential imaging involves observing a target at different parallactic or orientation angles, subtracting the PSF, then rotating the images to the same angle and combining them to enhance the signal of a planet. So PynPoint looks for the parallactic angle to perform this rotating and combining. We modified the code slightly to direct PynPoint to the HST orientation angle instead. Because of ACS's geometric distortion, however, we processed images of different orientations separately. This also allows for possible confirmation of any supposed planets by seeing if they appear in both orientations, though the absence of a source in only one orientation does not preclude its reality as a planet; we will discuss this further in section 4.2.

There are various options available in PynPoint to help optimize PSF subtraction. We mention a few that we use here and refer the reader to Amara et al. (2015) as well as the PynPoint website for a more complete description.

Although Amara et al. (2015) instruct that the input images should already be aligned, there is an option in PynPoint called `recent` that will further recenter the images. This can be helpful to fine tune the alignment, and in our experience it does appear to give a better subtraction. However, we also noticed that while it aligned the images with each other, it seemed to offset them from the center of the PynPoint window by a few pixels. The reasons for this still elude us. This is not really

problematic for the subtraction, but does add a kink in trying to determine the locations of sources found. There is also an option to rescale the images with the `resize` option. This allows PynPoint to recover subpixel information about the PSF (Amara & Quanz 2012). The degree of rescaling is set by the user; we doubled the resolution of our images by rescaling by a factor of 2, as in Amara & Quanz (2012). The user can also specify the size of the mask used to block out the center of the PSF. As described by Amara & Quanz (2012), this can be useful because the PSF core may be saturated and thus not contain useful information about the shape of the PSF. We decided not to block any of the image because we found that using different mask sizes did not seem to significantly affect our results.

3.3 Image Preparation and Using the Program

We went through several preliminary steps to ready the images for use with PynPoint. The data used with the program need to be calibrated for instrumental effects and corrected for cosmic rays. The crj images downloaded from the MAST archive are already bias, dark, and flat corrected, so we did not need to worry about that. They also come cosmic ray cleaned. This is important because not only could pixels hit by cosmic rays potentially affect the PSF modeling, but a cosmic ray can easily masquerade as a planet.

A crucial step in preparing the images for PynPoint is aligning them. Obviously, subtracting a misaligned PSF, or a PSF modeled from misaligned images, won't produce a good result. To perform the image alignment, we used the `imalign` command in IRAF. This command, as with most image alignment programs, is best suited to aligning fields with multiple stars visible, and thus having multiple references for the alignment. With images of many different fields, we had to rely on aligning features of the PSF, primarily the bright core. Further alignment was also done with the `recent` option in PynPoint. Although this offset all the images from the center of the window, it

did improve the PSF subtraction.

After the images were processed with `imalign`, we trimmed them to the arbitrary size of 60 $\times$ 60 pixels, centered on the star, following the example of Amara & Quanz (2012). We also used the `resize` option in PynPoint to scale the images up by a factor of 2. The final images used in the analysis were thus 120 $\times$ 120 pixels with a field of view of roughly 1.68" $\times$ 1.5".

We defined instances of the `images` class as all the available crj images for a target of interest. Our basis was all the aligned and trimmed crj images for the F606W filter in the HST archive, the bad frames having been removed. In total, this was 185 images. The basis included the images of the target. This may be of some concern, since with the target data in the basis the program may include any planets in the model and then subtract them out. However, Amara & Quanz (2012) found that this is not really an issue. Our experience validates this conclusion, evidenced by the results presented in Chapter 4.

For each of our targets, we ran PynPoint while varying the number of PCA coefficients used from 10 to 180, in steps of 10. We visually inspected each residuals image for any sources that stood out. The PSF subtraction can often leave behind residual speckles that look like real companions. To distinguish between real and fake sources, we noted the strength of each source compared to other residual features as well as the persistence of each source with different numbers of PCA coefficients. Real companions will consistently show up in the same location in the residuals images for a wide range of PCA coefficients. Artificial speckles generally will not show up in as many residuals images and, depending on the quality of the subtraction, may get removed completely with the optimum number of PCA coefficients while a real source remains. Additionally, a real companion should appear as a point source in the image (possibly combined with an extended emission component, e.g. as in Quanz et al. 2013), while other residual patterns may appear just extended.

For targets in which a notable point source appeared, we ran the corresponding drz images in

PynPoint. While the drz frames are not cosmic-ray cleaned – and, in our experience, didn't seem to produce as good of a subtraction as the crj images – the fact that they are distortion-corrected meant we could use them to get accurate positions of the objects seen. We processed the drz images the same way as the crj frames and each time found the corresponding point sources in the PSF-subtracted images. From this we determined the angular separations and position angles, measured east of north, of the sources.

Chapter 4

Results

4.1 Behind the Coronagraph

ACS's coronagraph is large. At 0.9" in radius, it blocks much of a target star's environment. How could we hope to see anything close enough to the star that it might actually be associated with it?

Even though the target star is behind the mask, its light still gets scattered about the coronagraph. In the case of the ACS coronagraph, there is a central peak in brightness that appears at the location of the star (Krist 2000). Since the planetary companions we would hope to find are point sources like their host stars, we would expect them to behave in the same way. Therefore, it is theoretically possible to detect planetary point sources even if they are located behind the coronagraph.

4.2 Recovery of HD 100546 b and c

The presence of HD 100546 images in the coronagraphic F606W dataset provided a good opportunity to test our method by seeing if we could recover the known planet and/or the candidate second companion. It was observed under HST proposal 9295 with Holland Ford as P.I. The ACS F606W images were taken March 26, 2003, while the HD 100546 b discovery data of Quanz et al. (2013)

were obtained May 30, 2011. Their observations showed the planet at a separation of ~ 0.48" and position angle of $\sim 8.9°$. For a physical separation of 53 AU (Quanz et al. 2015) and assuming a circular orbit, we calculate that during this time interval, the planet would have moved just less than 12° along its deprojected orbit. The recent Gaia data release shows HD 100546 to be a bit farther than the distance used in Quanz et al. (2015), and thus the planet's orbital radius is larger as well. Considering this as well as projection effects, the actual predicted difference in position between 2003 and 2011 is most likely less than what we calculated.

Data on HD 100546 are from two different telescope orientations, 179.05° and -152.95°, that we processed separately because of ACS's geometric distortion. There were two crj images per orientation. In the residuals image for the data taken at 179.05°, we detected a source located north of the central star for a wide range of PCA coefficients. We determined it to be 0.35" away from the star with a position angle of 6°. This separation is a bit smaller than what other observations have found, but the position angle is consistent with where we might expect the planet to be. To determine the signal-to-noise ratio (S/N), we used Equation (9) in Mawet et al. (2014). We found a S/N for this source of 3.2.

We do not see this object in the -152.95° residuals image. However, we do notice a source 0.20" from the star at a position angle of 64°, with a S/N of 4.2. This could possibly be the second candidate object, HD 100546 c, originally detected by Currie et al. (2015) at ~ 0.13" from the star. Naturally, the next question is why we don't see both objects in both orientations. A possible explanation is the fact that the ACS PSF is not axisymmetric. Some parts are brighter and some are dimmer. Thus, it may very well be that some portions are easier for PynPoint to model than others, and likewise a faint companion will show up more easily at some positions than at others. It could be that each telescope orientation placed one, but not both, of the planets at a favorable location within the PSF. We present the PSF subtracted images for both orientations in Figure 4.1.

To further confirm the reality of the detection of HD 100546 b, we downloaded ACS HRC

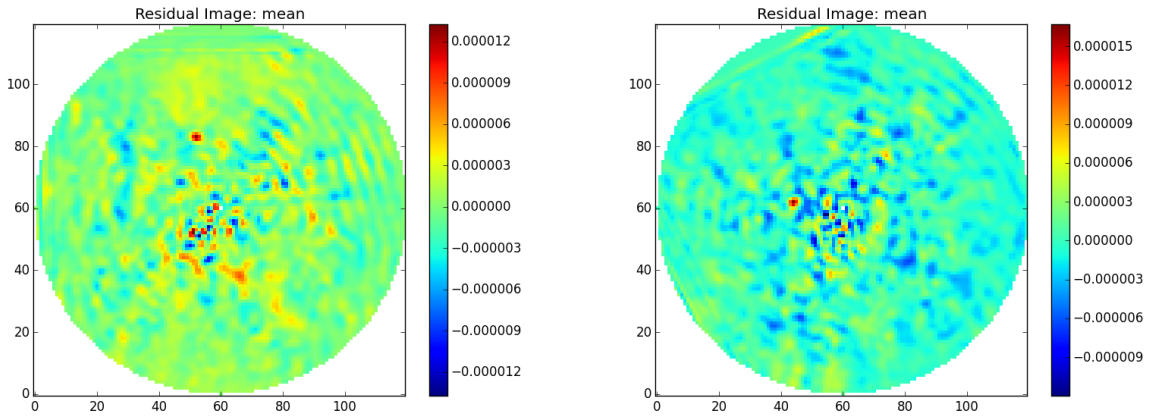

Figure 4.1 PynPoint residuals images of HD 100546, showing what we think may be the known planet (left) and the candidate second object (right), in the first and second orientations, respectively. The color bars to the right are arbitrary linear scales. North is up and east is to the left.

coronagraphic data taken in the F814W filter. There aren't nearly as many of these images available for making a basis as there are F606W images. Of our F606W targets of interest, only HD 100546, HD 141569, and HD163296 have F814W data, and these were taken at the same times and orientation angles as their F606W counterparts. After removing bad acquisitions, there were only 45 images left to constitute the basis. We aligned and trimmed the data in the same manner as we did the F606W data.

Oddly, the subtractions with PynPoint reveal a source at 0.35" and 6°, but in the -152.95° data, not 179.05° where it is seen in the F606W residuals image. We confirmed that there was not a mix-up in the image header information by comparing the positions of other field stars in the pre-trimmed images. A likely explanation, we think, is that we do not have enough basis images in the F814W filter to yield a very good subtraction, and we need to investigate this further. According to Choquet et al. (2014), with PCA algorithms, if there is a companion in a reference image, it can appear in the PSF-subtracted science image as a positive artifact. Since the HD 100546 images are in the PynPoint basis, and given the paucity of F814W basis images, we think this is why the object

shows up in the -152.95° residuals image and not the other orientation.

We consider other possibilities for the point source we detect.

-Since we see it in the two independent data sets of the F606W and F814W filters, it is extremely unlikely that both sources are cosmic rays.

-If it were an artifact introduced by a problem or inadequacy in the PSF subtraction, we would expect to see similar artifacts in the residuals images for other targets, which we do not.

-Similarly, if it were some sort of instrumental or coronagraphic artifact, we would expect to see it in the F606W data from both telescope orientations, as well as in the residuals images of other targets that were observed around the same time. We do not.

-If real, the source could still be a background star. However, its proximity to the expected planet position leads us to believe otherwise.

The most likely explanation, we believe, is that it is indeed the planet, but we'll need to further explore why we didn't detect it at both orientations.

4.3 Nondetections

HD 34282 and HD 97048 were both observed under HST proposal 10425 with P.I. Margaret Meixner, HD 34282 on January 10, 2005, and HD 97048 on July 16, 2005. There are two crj images available for each. We detect no sources in the vicinity of either of these. There was nothing particularly unusual or problematic about the analysis of these images, and the exposure times of the original frames are comparable to those of our other targets. HD 34282 is the most distant of our targets, so it may be particularly difficult to detect anything in its disk. We present residuals images for these stars in Figure 4.2.

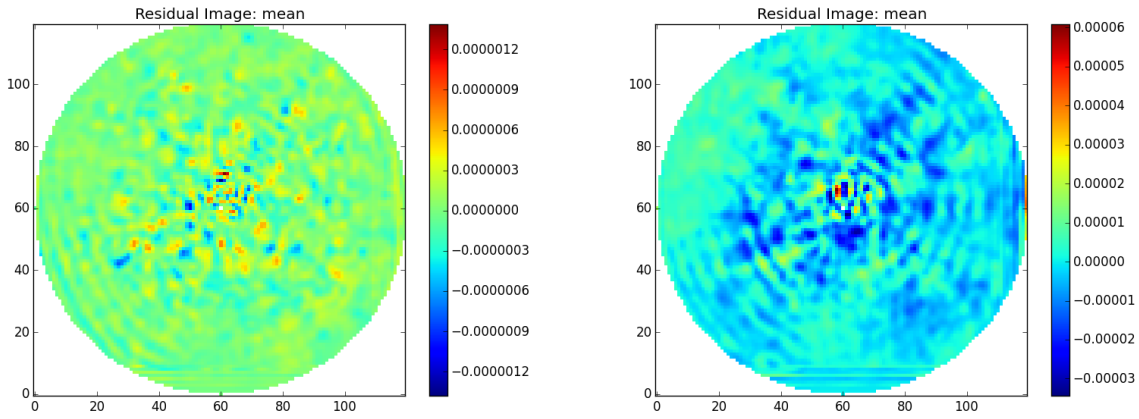

Figure 4.2 PSF subtracted images of HD 34282 on the left and HD 97048 on the right. We do not detect any new sources in these fields.

4.4 HD 100453

This star was observed on November 12, 2003, for HST proposal 9987 with P.I. Holland Ford. In the PSF-subtracted image, we clearly see something at a position angle of $\sim 22°$ and radius of ~ 0.7" from the central star. This is similar to the position given for "star C" in Collins et al. (2009), and we believe that object is what we have recovered. The field of view of our trimmed images is just slightly too small for us to see the M-dwarf companion HD 100453B, though it is obvious in the untrimmed images even without PSF subtraction. We do not observe any other sources in this field. However, there was only one image available; it is possible that something else would have shown up if there were more frames. The residuals image for this star is in the top left panel of Figure 4.3.

4.5 HD 141569

HD 141569 was observed at two orientations on July 21, 2002, under HST proposal 8992 with P.I. Holland Ford. There is only one crj frame per orientation for this object. In the first residuals image, we detect a fairly strong source at 0.55" and 156°. For a distance of 116 pc, this object

would be at a projected orbital radius of about 64 AU. We do not see anything in the image for the second orientation, or in the F814W data. However, this doesn't mean the first object is not real, as discussed above. We calculate a S/N of 7.1 for the source. The residuals image for the first orientation is shown in the top right of Figure 4.3.

4.6 HD 163296

HD 163296 had also been observed at two orientation angles, for which there are two frames each. The data were taken on March 25, 2003, for HST proposal 9295 with P.I. Holland Ford. In this case, we do see something in both residuals images, though they are at different enough locations that they are not the same object. We calculate the positions of the sources to be 0.36" and 164° for the first orientation and 0.45" and 95° for the second. We determine S/N values of 8.9 and 5.7, respectively, for these objects.

It is possible that one of these objects may account for one of the dust gaps observed by Isella et al. (2016). An angular radius of 0.36" amounts to a projected separation of about 44 AU for a distance of 122 pc. The second object would be at a projected distance of 55 AU. Accounting for projection effects due to disk inclination may place one of these at the predicted 60 AU. However, the gap at 60 AU was the one in which Isella et al. (2016) did not observe a depletion of gas and which they thus concluded was not likely caused by a planet. More observations are needed to determine the true nature of these sources and their influence on the disk structure. We do not see anything in the F814W residuals images for this target. In the bottom two panels of Figure 4.3 we present the PSF subtracted images for HD 163296, with the first orientation on the left and the second orientation on the right.

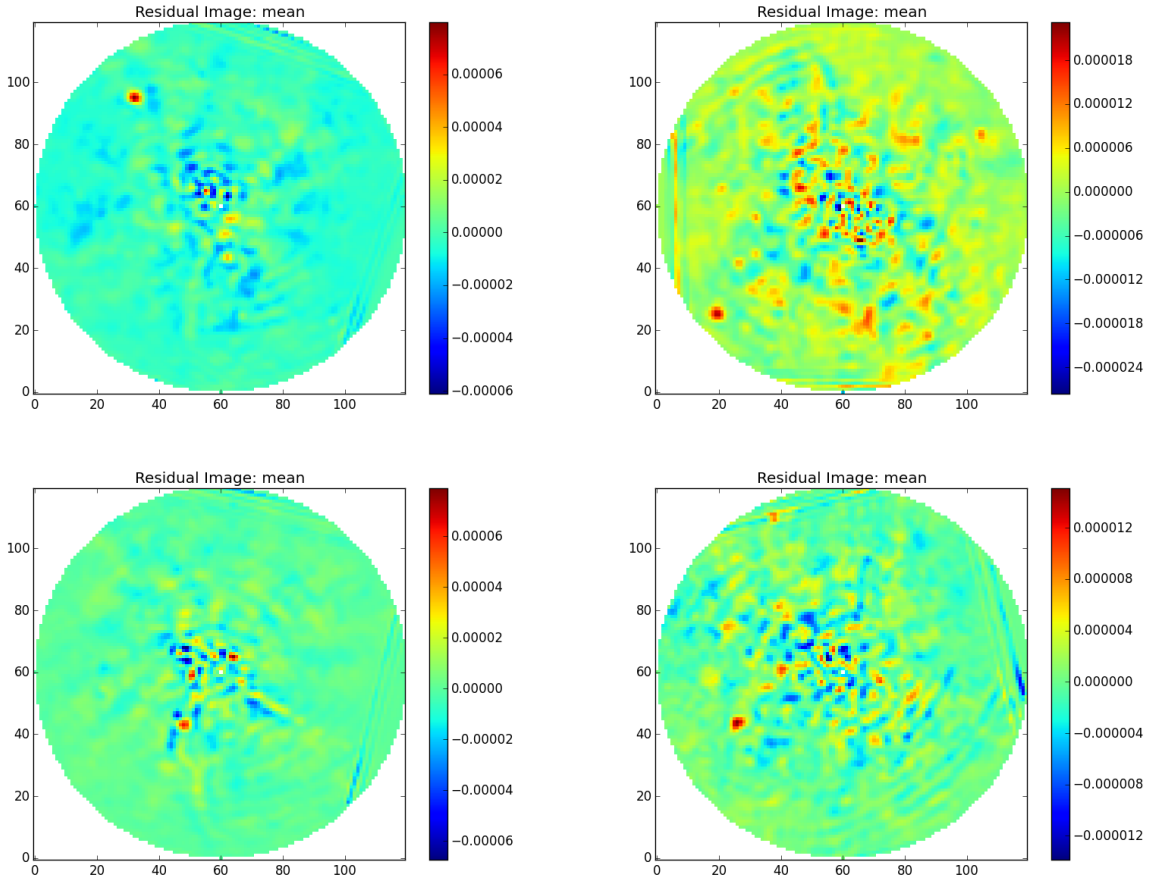

Figure 4.3 PynPoint residuals images of other targets in which we see point sources. All images have been rotated so north is up and east is to the left, and the color bars are arbitrary linear scales. Top left: HD 100453, with what is most likely "star C". Top right: HD 141569, with an object in the lower left. Bottom left: first orientation image of HD 163296. Bottom right: second orientation image of HD 163296.

4.7 Concluding Remarks

The new sources we have found are only candidates at this point. They will need to be confirmed via further observations to make sure they are not instrument artifacts and to establish common proper motion with their host stars. If real companions, they will warrant further multiwavelength observations that will provide valuable insights into how planets can form and influence disks.

It should also be noted that if they are real planets, they would almost certainly be too cold to show up in their own thermal emission in our results here. What we would be seeing is light reflected from the central star. The amount of incident light that is reflected off a planet depends on both the size and albedo of said object. Thus, studying this aspect may yield information about the radius and composition of the planet.

One way to try to determine the reality of these sources may be to measure their magnitude contrast with the central stars. Those calculations are beyond the scope of this project but are the next step. Using an estimate for the radius of the supposed planet and an albedo similar to Jupiter's, we can get an idea of how much reflected light we should be able to see. We can then compare this with the magnitude that we measure.

We would also like to point out that although we didn't see any new candidate planets around HD 34282, HD 97048, or HD 100453, this doesn't mean that the planets don't exist. There could still be objects in the disks of these stars that just aren't bright enough to be seen in our work here. If our detections are real, we have detected candidates in 40% of the disks surveyed that were not already known to have a planet, which is a significant percentage, albeit five stars is not a significant sample size.

This work has focused on HAeBe stars. However, these are of course not the only targets in the dataset we used. It would be worthwhile to similarly analyze the other objects in the dataset as they too may yield interesting information. Additionally, there are other filters of ACS and other instruments that have need of reprocessing with advanced techniques. These may yield still more

new candidates as well as confirm and provide more information about objects previously detected. They will also complement the results from new high-contrast imagers to help give a more complete picture of planet formation.

Bibliography

Acke, B., & van den Ancker, M. E. 2006, A&A, 449, 267

Alecian, E., Wade, G. A., Catala, C., et al. 2013, MNRAS, 429, 1001

Amado, P. J., Moya, A., Suárez, J. C., et al. 2004, MNRAS, 352, L11

Amara, A., & Quanz, S. P. 2012, MNRAS, 427, 948

Amara, A., Quanz, S. P., & Akeret, J. 2015, Astronomy and Computing, 10, 107

Ardila, D. R., Golimowski, D. A., Krist, J. E., et al. 2007, ApJ, 665, 512

Augereau, J. C., Lagrange, A. M., Mouillet, D., & Ménard, F. 1999, A&A, 350, L51

Augereau, J. C., Lagrange, A. M., Mouillet, D., & Ménard, F. 2001, A&A, 365, 78

Avila, R., et al. 2017, ACS Instrument Handbook, Version 16.0 (Baltimore: STScI)

Benisty, M., Tatulli, E., Ménard, F., & Swain, M. R. 2010, A&A, 511, A75

Biller, B. A., Liu, M. C., Rice, K., et al. 2015, MNRAS, 450, 4446

Borucki, W. J., Koch, D., Basri, G., et al. 2010, Science, 327, 977

Casey, M. P., Zwintz, K., Guenther, D. B., et al. 2013, MNRAS, 428, 2596

Chen, P. S., Shan, H. G., & Zhang, P. 2016, New Ast., 44, 1

Chen, X. P., Henning, T., van Boeckel, R., & Grady, C. A. 2006, A&A, 445, 331

Choquet, É., Pueyo, L., Hagan, J. B., et al. 2014, Proc. SPIE, 9143, 57

Cieza, L. A. 2016, IAU Symposium, 314, 128

Collins, K. A., Grady, C. A., Hamaguchi, K., et al. 2009, ApJ, 697, 557

Currie, T., Cloutier, R., Brittain, S., Grady, C., Burrows, A., Muto, T., Kenyon, S. J., & Kuchner, M. J. 2015, ApJL, 814, L27

Currie, T., Grady, C. A., & Cloutier, R. 2016, ApJL, 819, L26

Dent, W. R. F., Greaves, J. S., & Coulson, I. M. 2005, MNRAS, 359, 663

Dong, R., Zhu, Z., Fung, J., et al. 2016, ApJL, 816, L12

Folsom, C. P., Bagnulo, S., Wade, G. A., et al. 2012, MNRAS, 422, 2072

Fukagawa, M., Tamura, M., Itoh, Y., et al. 2010, PASJ, 62, 347

Fung, J., & Dong, R. 2015, ApJL, 815, 2

Gaia Collaboration. 2016, yCat, Gaia DR1

Garufi, A., Quanz, S. P., Schmid, H. M., et al. 2014, A&A, 568, A40

Gaudi, B. S., Stassun, K. G., Collins, K. A., et al. 2017, Nature, 546, 514

Ginski, C., Stolker, T., Pinilla, P., et al. 2016, A&A, 595, A112

Gomez Gonzalez, C. A., Absil, O., Absil, P. A., et al. 2016, A&A, 589, A54

Grady, C. A., Devine, D., Woodgate, B., et al. 2000, ApJ, 544, 895

Grady, C. A., Polomski, E. F., Henning, T., et al. 2001, AJ, 122, 3396

Guidi, G., Tazzari, M., Testi, L., et al. 2016, A&A, 588, A112

Guimarães, M. M., Alencar, S. H. P., Corradi, W. J. B., & Vieira, S. L. A. 2006, A&A, 457, 581

Habart, E., Testi, L., Natta, A., & Carbillet, M. 2004, ApJ, 614, 129

Houk, N., & Cowley, A. P. 1975, Michigan Catalogue of Two-Dimensional Spectral Types for the HD Star

Isella, A., Guidi, G., Testi, L., et al. 2016, PRL, 117, 251101

Isella, A., Testi, L., Natta, A., et al. 2007, A&A, 469, 213

Juhász, A., Bouwman, J., Henning, T., et al. 2010, ApJ, 721, 431

Keller, L. D., Sloan, G. C., Forrest, W. J., et al. 2008, ApJ, 684, 411

Khalafinejad, S., Maaskant, K. M., Mariñas, N., & Tielens, A. G. G. M. 2016, A&A, 587, A62

Kraus, A. L., & Ireland, M. J. 2012, ApJ, 745, 5

Krist, J. 2000, The predicted performance of the ACS coronagraph, Tech. rep.

Kuhn, J. R., Potter, D., & Parise, B. 2001, ApJ, 553, L189

Lafrenière, D., Marois, C., Doyon, R., Nadeau, D., & Artigau, É. 2007, ApJ, 660, 770

Lagage, P. O., Doucet, C., Pantin, E., et al. 2006, Science, 314, 621

Lagrange, A. M., et al. 2009, A&A, 493, L21

Levenhagen, R. S., & Leister, N. V. 2006, MNRAS, 371, 252

Lindegren, L., Lammers, U., Bastian, U., et al. 2016, A&A, 595, A4

Long, Z. C., Fernandes, R. B., Sitko, M., et al. 2017, ApJ, 838, 62

Maaskant, K. M., Honda, M., Waters, L. B. F. M., et al. 2013, A&A, 555, A64

Marois, C., Doyon, R., Racine, R., & Nadeau, D. 2000, PASP, 112, 91

Marois, C., Lafrenière, D., Doyon, R., Macintosh, M., & Nadeau, D. 2006, ApJ, 641, 556

Mawet, D., Milli, J., Wahhaj, Z., et al. 2014, ApJ, 792, 97

McCaughrean, M. J., & O'dell, C. R. 1996, AJ, 111, 1977

Merín, B., Montesinos, B., Eiroa, C., et al. 2004, A&A, 419, 301

Monnier, J. D., Harries, T. J., & Aarnio, A. 2017, ApJ, 838, 20

Mouillet, D., Lagrange, A. M., Augereau, J. C., & Ménard, F. 2001, A&A, 372, L61

Pantin, E., Waelkens, C., & Lagage, P. O. 2000, A&A, 361, L9

Piétu, V., Dutrey, A., & Kahane, C. 2003, A&A, 398, 565

Pineda, J. E., Quanz, S. P., Meru, F., et al. 2014, ApJL, 788, L34

Quanz, S. P., Amara, A., Meyer, M. R., Girard, J. H., Kenworthy, M. A., & Kasper, M. 2015, ApJ, 807, 64

Quanz, S. P., Amara, A., Meyer, M. R., Kenworthy, M. A., Kasper, M., & Girard, J. H. 2013, ApJL, 766, L1

Racine, R., Walker, G. A. H., Nadeau, D., Doyon, R., & Marois, C. 1999, PASP, 111, 587

Rameau, J., Chauvin, G., Lagrange, A. M., et al. 2013, ApJL, 779, L26

Seok, J. Y., & Li, A. 2017, ApJ, 835, 291

Smith, B. A., & Terrile, R. J. 1984, Science, 226, 1421

Smith, L. I. 2002, A tutorial on Principal Components Analysis

Soummer, R., Pueyo, L., & Larkin, J. 2012, ApJL, 755, L28

Uyama, T., Hashimoto, J., Kuzuhara, M., et al. 2017, AJ, 153, 106

van Boeckel, R., Min, M., Waters, L. B. F. M., et al. 2005, A&A, 437, 189

van den Ancker, M. E., de Winter, D., & Tjin A Djie, H. R. E. 1998, A&A, 330, 145

van den Ancker, M. E., The, P. S., Tjin A Djie, H. R. E., et al. 1997, A&A, 324, L33

van der Plas, G., Wright, C. M., Ménard, F., et al. 2017, A&A, 597, A32

Wagner, K., Apai, D., Kasper, M., & Robberto, M. 2015, ApJL, 813, L2

Walsh, C., Juhász, A., Meeus, G., et al. 2016, ApJ, 831, 200

Wang, J. J., Ruffio, J. B., De Rosa, R. J., Aguilar, J., Wolff, S. G., & Pueyo, L. 2015, pyKLIP: PSF Subtraction for Exoplanets and Disks, Astrophysics Source Code Library

Weinberger, A. J., Becklin, E. E., Schneider, G., et al. 1999, ApJ, 525, L53

Weinberger, A. J., Rich, R. M., Becklin, E. E., Zuckerman, B., & Matthews, K. 2000, ApJ, 544, 937

Williams, J. P., & Cieza, L. A. 2011, ARA&A, 49, 67